

# Boron Phosphide Films by Reactive Sputtering: Searching for a P-Type Transparent Conductor

Andrea Crovetto,\* Jesse M. Adamczyk, Rekha R. Schnepf, Craig L. Perkins, Hannes Hempel, Sage R. Bauers, Eric S. Toberer, Adele C. Tamboli, Thomas Unold, and Andriy Zakutayev\*

With an indirect band gap in the visible and a direct band gap at a much higher energy, boron phosphide (BP) holds promise as an unconventional p-type transparent conductor. This work reports on reactive sputtering of amorphous BP films, their partial crystallization in a P-containing annealing atmosphere, and extrinsic doping by C and Si. The highest hole concentration to date for p-type BP ( $5 \times 10^{20} \text{ cm}^{-3}$ ) is achieved using C doping under B-rich conditions. Furthermore, bipolar doping is confirmed to be feasible in BP. An anneal temperature of at least 1000 °C is necessary for crystallization and dopant activation. Hole mobilities are low and indirect optical transitions are stronger than that predicted by theory. Low crystalline quality probably plays a role in both cases. High figures of merit for transparent conductors might be achievable in extrinsically doped BP films with improved crystalline quality.

eral applications such as a corrosion- and heat-resistant coating,<sup>[4,5]</sup> photo- and electrocatalyst,<sup>[6,7]</sup> as well as for thermal management<sup>[1]</sup> and extreme UV optics applications.<sup>[8]</sup> More recently, BP was identified as a potential p-type transparent conductive material (TCM).<sup>[9]</sup> This is a particularly interesting prospect, because obtaining high p-type conductivity in optically transparent materials is still an unsolved challenge.<sup>[10,11]</sup> Unlike the case of other p-type TCM candidates, bipolar doping has been reported in BP by various authors.<sup>[3,5,9,12,13]</sup> Thus, BP could be a unique example of a transparent material with both p-type and n-type doping capability.

## 1. Introduction

Numerous III-V semiconductors such as GaAs, InP, GaN, and related alloys are technologically mature materials. They are key components of optoelectronic devices such as light-emitting diodes, photodetectors, lasers, and high-efficiency solar cells. Boron phosphide (BP) is a relatively under-investigated member of this family in spite of its ultra-high thermal conductivity,<sup>[1]</sup> chemical inertness and hardness,<sup>[2]</sup> and prospects for bipolar doping.<sup>[3]</sup> Accordingly, BP has been proposed for sev-


eral applications such as a corrosion- and heat-resistant coating,<sup>[4,5]</sup> photo- and electrocatalyst,<sup>[6,7]</sup> as well as for thermal management<sup>[1]</sup> and extreme UV optics applications.<sup>[8]</sup> More recently, BP was identified as a potential p-type transparent conductive material (TCM).<sup>[9]</sup> This is a particularly interesting prospect, because obtaining high p-type conductivity in optically transparent materials is still an unsolved challenge.<sup>[10,11]</sup> Unlike the case of other p-type TCM candidates, bipolar doping has been reported in BP by various authors.<sup>[3,5,9,12,13]</sup> Thus, BP could be a unique example of a transparent material with both p-type and n-type doping capability.

BP crystallizes in the diamond-derived zincblende structure with tetrahedral coordination. Because the electronegativity difference between B and P is small, BP is a covalent solid and its band structure is closely related to that of Si and C in the diamond structure. The main difference is an intermediate size of the fundamental indirect band gap for BP ( $\approx 2.0 \text{ eV}$ )<sup>[14–16]</sup> mainly due to an intermediate bond length. Although this band gap corresponds to visible light, the direct band gap of BP is much wider and falls in the UV region ( $\approx 4.3 \text{ eV}$ ).<sup>[15–17]</sup> The weakness of indirect transitions predicted for BP at room temperature<sup>[15]</sup> is the key factor that could make BP thin films sufficiently transparent for many TCM applications. For example, a 100 nm-thick BP film is expected to absorb negligible amounts of red-yellow light and less than 10% of violet light according to first-principles calculations including electron-phonon coupling.<sup>[15]</sup> With respect to electrical properties, BP has a highly disperse valence band produced by p orbitals, ensuring low hole effective masses ( $0.35 m_e$ ).<sup>[9]</sup> Unlike the case of diamond, the valence band maximum of BP lies at a relatively shallow energy with respect to the vacuum level. Shallow, disperse valence bands are usually uncorrelated with high p-type dopability, due to easier formation of uncompensated shallow acceptor defects.<sup>[18,19]</sup>

A. Crovetto, R. R. Schnepf, C. L. Perkins, S. R. Bauers, A. C. Tamboli, A. Zakutayev  
Materials Science Center  
National Renewable Energy Laboratory  
Golden, CO 80401, USA  
E-mail: andriy.zakutayev@nrel.gov

A. Crovetto, H. Hempel, T. Unold  
Department of Structure and Dynamics of Energy Materials  
Helmholtz-Zentrum Berlin für Materialien und Energie GmbH  
14109 Berlin, Germany  
E-mail: andrea.crovetto@helmholtz-berlin.de

J. M. Adamczyk, R. R. Schnepf, E. S. Toberer, A. C. Tamboli  
Department of Physics  
Colorado School of Mines  
Golden, CO 80401, USA

 The ORCID identification number(s) for the author(s) of this article can be found under <https://doi.org/10.1002/admi.202200031>.

© 2022 The Authors. Advanced Materials Interfaces published by Wiley-VCH GmbH. This is an open access article under the terms of the Creative Commons Attribution License, which permits use, distribution and reproduction in any medium, provided the original work is properly cited.

DOI: 10.1002/admi.202200031

## 2. Open Questions in BP Research

### 2.1. Conductivity and Transparency

The highest conductivity reported for p-type BP is  $3600 \text{ S cm}^{-1}$  for a nominally undoped single-crystalline film deposited by chemical vapor deposition (CVD) at 1050 °C using  $\text{B}_2\text{H}_6$  and

PH<sub>3</sub> gas precursors in hydrogen, as reported by Shohnho et al.<sup>[3]</sup> Remarkably, this value is on par with the conductivities of the best n-type TCMs.<sup>[20]</sup> The hole concentration and mobility were  $8 \times 10^{19} \text{ cm}^{-3}$  and  $285 \text{ cm}^2 \text{ V}^{-1} \text{ s}^{-1}$ , respectively. However, intrinsic defects in BP are not expected to be effective dopants<sup>[9]</sup> so the origin of the high carrier concentration is unclear and requires further investigation. In addition, such a high conductivity has not been reproduced by others, with more commonly reported values being in the  $0.1\text{--}50 \text{ S cm}^{-1}$  range for both n-type and p-type BP.<sup>[2,5,13,21–23]</sup>

A common figure of merit (FOM) for TCMs is the ratio between electrical conductivity and average absorption coefficient in the visible.<sup>[20,24]</sup> However, the absorption coefficient of BP has rarely been measured. Absorption coefficients of single crystals and single-crystalline films<sup>[13,14,21]</sup> are generally below  $1 \times 10^3 \text{ cm}^{-1}$  at 2.5 eV, in line with computational predictions. Yet, a more recent measurement on a BP thin film<sup>[25]</sup> shows a substantially higher absorption coefficient, above  $1 \times 10^4 \text{ cm}^{-1}$  in most of the visible region. Furthermore, BP films on transparent substrates are usually described as orange,<sup>[22]</sup> red,<sup>[12]</sup> brown,<sup>[13]</sup> or black,<sup>[26]</sup> indicating that their optical transmission may not be sufficiently high.

The only case where electrical conductivity and absorption coefficient were measured on the same BP sample is the CVD-grown n-type single-crystalline BP film reported by Iwami et al.<sup>[13]</sup> with a FOM of  $\approx 0.02 \Omega^{-1}$ . If we use the absorption coefficient from this study to estimate the FOM of the most conductive p-type BP films reported by Shohnho et al.,<sup>[3]</sup> we get an FOM of  $1.8 \Omega^{-1}$ . To contextualize these values, the highest FOM we are aware of for a p-type TCM of any kind is  $1.3 \Omega^{-1}$  for reactively sputtered CuI.<sup>[27]</sup> Thus, BP deserves experimental scrutiny with focus on its applicability as a p-type TCM.

## 2.2. Film Growth

BP is notoriously difficult to synthesize due to the simultaneous presence of a highly inert (B) and a volatile species (P).<sup>[28]</sup> High growth temperatures (typically above  $900 \text{ }^\circ\text{C}$ ) are necessary to activate boron diffusion and obtain crystalline BP, but at these temperatures BP tends to decompose into boron-rich phosphides (such as B<sub>6</sub>P) and gaseous phosphorus.<sup>[3,29]</sup> For this reason, previous thin-film work on BP has given strong preference to CVD processes near atmospheric pressure where it is easier to prevent P losses by keeping a high P partial pressure during deposition. With CVD-based processes, it has been possible to grow BP up to  $1100\text{--}1200 \text{ }^\circ\text{C}$  depending on the precursors.<sup>[3,30]</sup> Attempts to grow BP in high vacuum by solid-source evaporation<sup>[31]</sup> and gas-phase molecular beam epitaxy<sup>[29]</sup> resulted in amorphous films and insufficient P incorporation at elevated temperatures. Sputter deposition could be a viable alternative because it operates under intermediate pressure conditions. As a non-equilibrium plasma-assisted process, sputter deposition may enable lower temperature growth<sup>[32]</sup> and higher dopant solubility in the host material<sup>[33]</sup> compared to thermal processes. Besides, epitaxial single-crystalline CVD films grown above  $1000 \text{ }^\circ\text{C}$  are of limited applicability in the TCM industry, where cost-effective large-area coating of glass substrates or multilayer stacks are necessary. Magnetron sputtering, on the other hand,

is the deposition method of choice for many n-type TCMs in the industry.<sup>[34–36]</sup> We are only aware of one previous attempt of sputter deposition of BP.<sup>[37]</sup> Optoelectronic characterization was not conducted and it is also unclear if the deposited films actually consisted of BP.

The goal of this work is to answer some of the important open questions elaborated in this section. First, we establish that amorphous BP films can be deposited by reactive sputtering and can be crystallized in a post-annealing step. Second, we find higher absorption coefficients than expected, possibly due to enhanced indirect transitions associated with imperfect crystallinity. Finally, we apply C doping to achieve bipolar conductivity and the highest hole concentration achieved so far in p-type BP. Thus, we confirm that BP can be doped both n-type and p-type, and we propose that BP may reach a high TCM FOM by a combination of high crystalline quality and extrinsic doping.

## 3. Results

### 3.1. One-Step Growth by Reactive Sputtering

Smooth amorphous BP films can be grown by reactive sputtering of B targets in a PH<sub>3</sub>/Ar atmosphere. The B/P ratio in the films, as measured by Auger electron spectroscopy (AES), can be continuously adjusted over a wide range at room temperature (Figure 1a). The main factor determining the B/P ratio at fixed temperature is the PH<sub>3</sub> partial pressure, with no

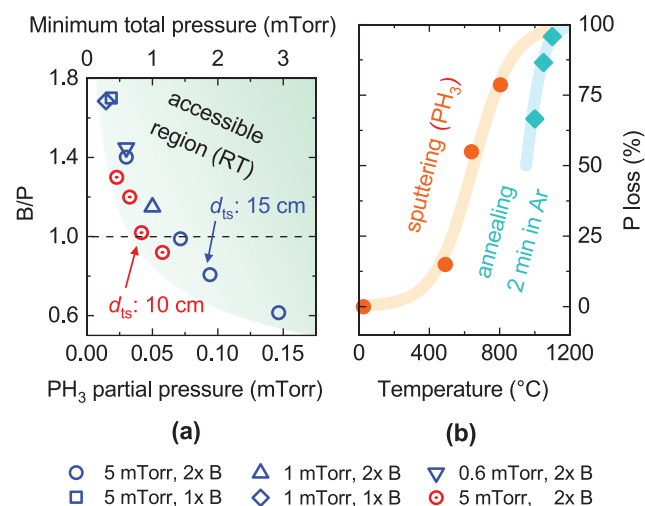


**Figure 1.** Composition of B-P films. a) Atomic B/P ratio of B-P films sputtered at room temperature versus PH<sub>3</sub> partial pressure. Datasets for two different target–substrate distances  $d_{ts}$  are shown. Different symbols refer to different total pressures and numbers of co-sputtering B targets (“2x B” meaning two targets). Assuming that the PH<sub>3</sub> concentration cannot exceed 5% of the Ar background, each PH<sub>3</sub> partial pressure has a corresponding minimum total pressure at which the B/P region below the data points is not experimentally accessible. b) Phosphorus loss in B-P films as a function of temperature. Circles refer to the decrease in P content as a function of sputter deposition temperature with respect to room temperature deposition under otherwise identical conditions. Diamonds refer to the P loss of B-P films annealed at 1 bar for 2 min under a continuous Ar flow. Lines are guides to the eye.

significant role played by the total sputter pressure and the number of simultaneously sputtering B targets (one or two). A typical oxygen content in the bulk is 2 at.% according to AES.

We infer from these observations that P incorporation in reactively sputtered BP neither occurs as a reaction at the target, nor as a direct reaction of  $\text{PH}_3$  with elemental B at the substrate (see Supporting Information). The most likely explanation is that  $\text{PH}_3$  cracks into more reactive species in the plasma region in front of each target, with subsequent condensation of P at the substrate. The wide continuous range of B/P ratios that can be achieved in the films indicates that P condensation at the substrate results in the formation of B–P bonds as well as P–P bonds. Due to the volatility of P at high temperatures (Figure 1b), a  $\text{PH}_3$  partial pressure of 0.4 mTorr is necessary to obtain B/P = 1 at a substrate temperature of 800 °C. Therefore, sputtering BP at very high temperatures requires either a high  $\text{PH}_3$  concentration in the sputter gas (beyond the 5% limit dictated by our pre-diluted  $\text{PH}_3$  bottle) or a high total sputter pressure.

Regardless of substrate temperature (25 to 800 °C) and stoichiometry ( $0.5 < \text{B/P} < 1.5$ ), the conductivity of all as-deposited BP films is too low to be measured on the plane of the substrate with a conventional four-point probe. An upper limit for their conductivity is about  $10^{-3} \text{ S cm}^{-1}$ , indicating that native defects (such as B and P antisites) are ineffective dopants in this temperature range. To check if these amorphous films could be crystallized, we conducted rapid thermal annealing (RTA) at atmospheric pressure under a continuous Ar flow. Despite the higher total pressure, the lack of a P partial pressure in the system led to rapid P losses. After 2 min at 1000 °C, the films have already lost 65% of their original P content (Figure 1b). Very short anneals at 1100 °C result in broad X-ray diffraction (XRD) peaks attributable to BP. However, the conductivity of all films after RTA is still below  $10^{-3} \text{ S cm}^{-1}$ . From these initial experiments, we conclude that annealing in a P-containing atmosphere is necessary to prevent P losses and explore a wider process window. It also seems unlikely that intrinsic doping can lead to significant carrier concentrations in BP, so options for extrinsic dopants should be explored.

### 3.2. Two-Step Growth by Reactive Sputtering and Annealing with Extrinsic Doping

To address the issues described above, we post-annealed BP films in sealed quartz ampoules in the presence of sacrificial red phosphorus powder. According to defect calculations, C and Si are the most attractive candidates for p-type doping of BP under B-rich conditions.<sup>[9]</sup> We found that C could be easily incorporated into BP by cleaning the ampoules with isopropyl alcohol before annealing (see Experimental Section). The C content of BP films annealed for 30 min is consistently in the 2.5–2.7 at.% range, roughly independent of annealing temperature. This extrinsic dopant concentration is similar to the case of n-type TCMs such as  $\text{ZnO:Al}$  and  $\text{In}_2\text{O}_3:\text{Sn}$ .<sup>[38,39]</sup> AES depth profiles indicate that the C impurities are homogeneously distributed throughout the depth of the films.

Raman spectra are very sensitive to C impurities in excess of their solubility in the BP matrix, due to the high scattering cross section of the D and G Raman bands in disordered

carbon.<sup>[43]</sup> Although these Raman bands are already detected at 2.5 at.% C in our samples (Figure S1, Supporting Information), this C impurity concentration is still sufficiently low not to have a significant effect on the optical properties of BP (Figure S2, Supporting Information). Based on an empirical relationship between the width of the D band and the C crystallite size,<sup>[43]</sup> we estimate that non-substitutional C segregates in very small clusters around 1 nm in size. Unless otherwise specified, the post-annealed BP films presented in the rest of the paper are C-doped. The annealing process also results in an increase of the O content in the bulk, from about 2% to about 6%. Two likely reasons are the incomplete removal of air when sealing the ampoules and the traces of isopropyl alcohol responsible for C doping. O impurities are unlikely to act as dopants in BP due to a large size mismatch with P.

With an annealing time of 30 min, a temperature of 900 °C is still not sufficient to detect any crystalline BP by XRD (Figure 2a). The corresponding Raman spectrum (Figure 2(b)) exhibits two broad bands centered at  $\approx 450 \text{ cm}^{-1}$  and  $\approx 700 \text{ cm}^{-1}$ . These could be attributed to the acoustic and optical phonon bands of zincblende BP with significant broadening.<sup>[15]</sup> However, the Raman features of amorphous red phosphorus<sup>[44]</sup> and amorphous B<sup>[45]</sup> are also located in these two spectral regions, so we cannot exclude the presence of the elemental forms of P and B. This film mainly consists of small ( $\approx 20 \text{ nm}$ ) particles, with some larger particles that appear brighter in the scanning electron microscope (SEM) and might therefore consist of elemental P (Figure 2c).

When the annealing temperature is increased to 1000 °C, a broad XRD peak with full width at half maximum (FWHM) of  $3.2^\circ 2\theta$  appears (Figure 2a). It can be attributed to the (111) reflection in zincblende BP. A similar peak FWHM is obtained after annealing at 1050 °C. Since these widths are much larger than instrumental broadening, and assuming that only size effects are responsible for broadening, we estimate a coherence volume of 3 nm using the Scherrer equation. This crystallite size is much smaller than the average particle size ( $\approx 30 \text{ nm}$ ) determined by SEM (Figure 2c) implying that each particle is poorly crystallized, although some medium-range order exists in some regions. In agreement with these observations, the Raman spectra of the films annealed at 1000 and 1050 °C for 30 min resemble the phonon density of states (DOS) calculated for BP.<sup>[15]</sup> The peaks at 804 and  $716 \text{ cm}^{-1}$  correspond to the two peaks in the optical phonon DOS. The peak at  $460 \text{ cm}^{-1}$  has a corresponding peak in the acoustic phonon DOS. We will refer to these films as nanocrystalline BP in the rest of the article.

To obtain higher crystalline quality, it is necessary to increase the annealing time. After a 24 h annealing at 1000 °C, all the main XRD peaks of zincblende BP can be detected with a FWHM of  $0.41^\circ 2\theta$  for the (111) reflection. Considering the Lorentzian broadening component of this peak and deconvolving instrumental broadening,<sup>[38,46]</sup> we estimate a crystallite size of 34 nm using the Scherrer equation. SEM images of this film (Figure 2c) show that the particle size is still in the 30 nm diameter range as for the films annealed for a shorter time, but the particle boundaries are much sharper. We conclude that long annealing times enable full crystallization of the (originally amorphous) BP particles, although the particles still do not coalesce into larger grains. The Raman spectrum of this sample



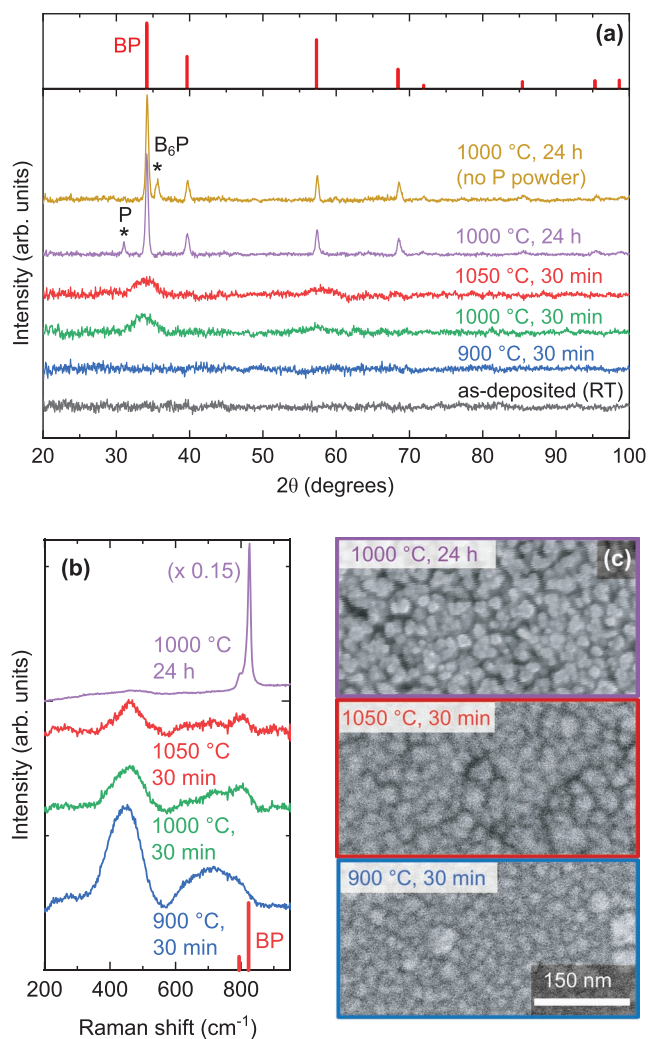


**Figure 2.** Structure and morphology of BP films. a) XRD patterns of various C-doped BP films annealed in sealed ampoules. Process conditions are indicated. The reference patterns for zincblende BP and rhombohedral  $B_6P$  are taken from the Inorganic Crystal Structure Database.<sup>[40,41]</sup> b) Raman spectra of four of the BP films shown in (a). The reference Raman spectrum of zincblende BP is shown.<sup>[42]</sup> c) SEM images of three of the BP films shown in (a).

(Figure 2b) is similar to spectra reported for high-quality BP crystals and single-crystalline films.<sup>[28,42,47]</sup> The main peak at  $827\text{ cm}^{-1}$  and the secondary peak at  $797\text{ cm}^{-1}$  can be attributed to the Raman-active longitudinal (LO) and transverse (TO) optical phonon modes at the  $\Gamma$  point, respectively.<sup>[15]</sup> Our 24 h long anneals result in phase segregation on the film surface, clearly visible in **Figure 3b**, and in a new XRD peak at  $31.0^\circ 2\theta$  (Figure 2a). According to AES imaging (Figure S3, Supporting Information), these surface secondary phases mainly consist of elemental P. The new XRD peak is compatible with both fibrous red phosphorus<sup>[48]</sup> and Hittorf's (violet) phosphorus.<sup>[49]</sup>

If red phosphorus powder is not present during annealing, part of BP decomposes into  $B_6P$  and gaseous P until the P partial pressure in the ampoule is sufficiently high to prevent further P evaporation. The occurrence of this reaction is confirmed by the XRD peak at  $35.5^\circ 2\theta$ , compatible with the

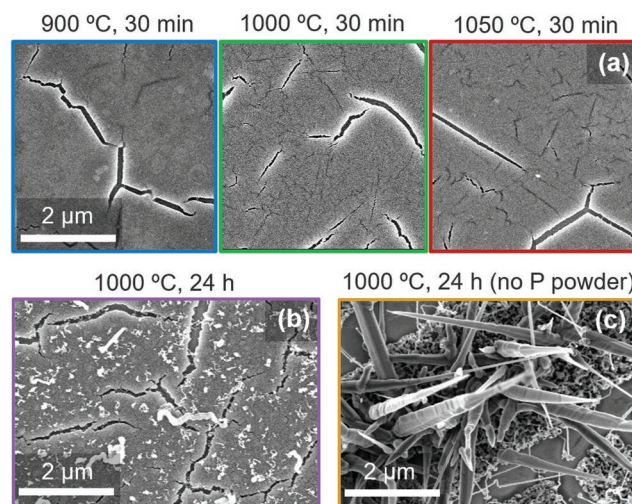


**Figure 3.** Low-magnification SEM images of the BP films shown in Figure 2a. a) Short anneals; b,c) Long anneals. All films except for (c) were annealed with sacrificial P powder. The secondary phases present in the film annealed for 24 h (b) are mainly elemental P. When no sacrificial P powder is present (c) a whisker morphology develops.

highest-intensity reflection of  $B_6P$ . A peculiar “whisker” morphology develops for some of the remaining BP in these films, with typical whisker diameters of roughly  $500\text{ nm}$  and lengths of a few  $\mu\text{m}$  (Figure 3c). BP whisker growth has sometimes been observed in CVD BP films.<sup>[22,50,51]</sup> Finally, we note that all the post-annealed BP films presented here exhibit cracks (Figure 3), probably due to the thermal expansion coefficient mismatch between BP and the fused silica substrate.<sup>[52]</sup>

### 3.3. Optical Properties

The absorption coefficient  $\alpha$  of the as-deposited films depends on their stoichiometry, with B-rich films having lower band gaps than B-poor films (Figure 4a). In these amorphous films,  $(\alpha h\nu)^n$  versus  $h\nu$  plots are roughly linear for  $1/3 < n < 1/2$  (Figure S4, Supporting Information), as usually found in amorphous semiconductors.<sup>[53]</sup> A similar spectral behavior and a decreasing band gap for increasing B content were found for amorphous  $B_xP$  films by CVD with  $x > 3$ .<sup>[30]</sup> The band gaps of the B-rich and the B-poor films are estimated as 1.3 and 2.0 eV, respectively (Figure S4, Supporting Information). Note that the calculated indirect band gap of crystalline BP is 1.98 eV using a hybrid exchange-correlation functional.<sup>[15]</sup>

The absorption coefficient of the amorphous as-deposited films is much larger than the computational prediction for perfectly crystalline BP below the direct band gap at 4 eV. This is expected because materials without long-range order do not require phonon participation in optical transitions. To achieve transparent conductivity in amorphous BP, a shift of the fundamental gap to higher photon energies with respect to the crystalline state would be advantageous to widen the transparency window. While this effect is very well known in amorphous Si,<sup>[54]</sup> we do not observe it in amorphous BP. In fact, a very recent molecular dynamics study predicts that amorphous BP should have an even lower band gap than crystalline BP.<sup>[55]</sup>

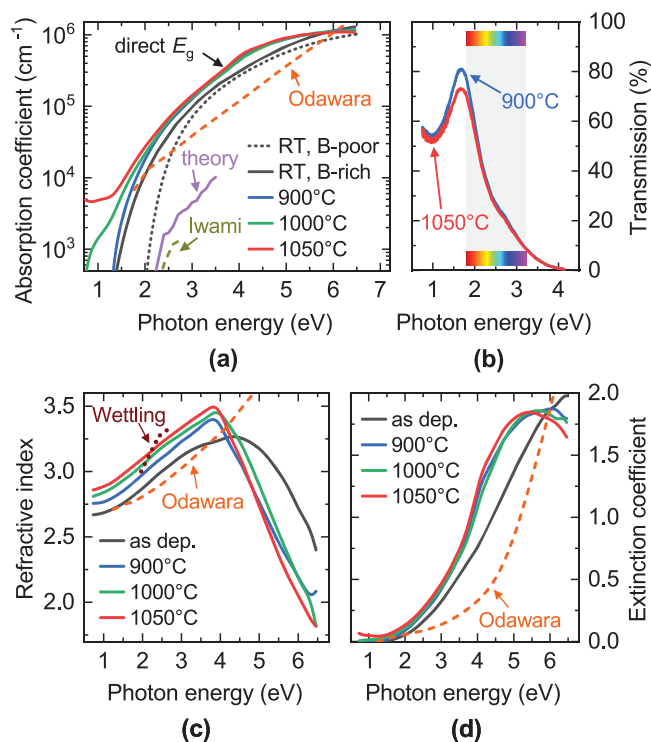


**Figure 4.** Optical properties of as-deposited BP (black lines) and post-annealed BP (colored solid lines, 30 min annealing). a) Absorption coefficient of B-rich films (B/P = 1.3, solid lines) and a B-poor as-deposited film (B/P = 0.6, dotted line). Post-annealed films were all obtained from the B-rich film. They reach a nearly stoichiometric composition after annealing. The computed absorption coefficient using a hybrid exchange correlation functional and electron-phonon coupling is shown.<sup>[15]</sup> Two previously measured absorption coefficients for BP films<sup>[13,25]</sup> are also shown. b) Optical transmission of two BP films annealed at different temperatures. c,d) Refractive index and extinction coefficient. The displayed films are the same as in (a). An additional experimental reference for the refractive index<sup>[57]</sup> is included.

The reason is that even short-range order is often broken in amorphous BP, with abundant homoelement bonds (B–B and P–P) occurring in B-rich and B-poor clusters. As the band gap of amorphous boron is 1.0 eV,<sup>[56]</sup> the B-rich clusters are likely responsible for band gap narrowing in amorphous BP, as well as its further narrowing under B excess.<sup>[30]</sup> Since this effect is unique to compound semiconductors, it may explain the discrepancy between the optical properties of amorphous BP and amorphous Si, in spite of their similar bonding and electronic structure in the crystalline state.

As shown in the next section and as observed by other workers,<sup>[3,5,9]</sup> B-rich conditions are necessary to achieve appreciable p-type conductivity in BP. Therefore, the remaining optical characterization shown in Figure 4 focuses on B-rich films with B/P = 1.3. We limit our study to the nanocrystalline films annealed for 30 min, because longer anneals generate very rough films with secondary phases (Figure 3b), so their optical characterization is not reliable. The absorption coefficient of the post-annealed films is overall slightly larger than in the as-deposited film (Figure 4a). The post-annealed films also have a secondary absorption onset in the 4.0–4.5 eV range (Figure S4, Supporting Information) which is absent from the

as-deposited films. This secondary onset is likely associated with the direct band gap of BP, predicted to lie at 4.34 eV from computation<sup>[15]</sup> and measured at 4.25 eV on crystalline BP.<sup>[17]</sup> The primary absorption onset appears to shift to lower photon energies with increasing annealing temperature, although this effect might be an artifact often seen in rough films due to scattering and/or depolarization effects.<sup>[58–60]</sup> In any case, the visible absorption coefficient of our post-annealed films is over one order of magnitude larger than the absorption coefficient computed for pristine BP<sup>[15]</sup> and is also significantly larger than the experimental absorption coefficient determined for an epitaxial CVD film by ellipsometry (Figure 4a).<sup>[25]</sup> As a consequence, the optical transmission of our ≈130-nm-thick films drops to very low values in the blue region of the visible (Figure 4b).

The refractive indices of our films match previous measurements on crystalline BP films<sup>[25,57]</sup> in the spectral region below the direct gap (Figure 4c). First-principles calculations using the Bethe–Salpeter equation on  $G_0W_0$  band structures also yield a similar refractive index in the visible part of the spectrum.<sup>[16]</sup> At higher photon energies, the refractive indices of our films decrease due to the inflection point in the extinction coefficient (Figure 4d). The slight increase in the refractive index and extinction coefficient with increasing annealing temperature is probably due to film densification upon annealing (see Supporting Information). By extrapolating the real part of the complex dielectric function to zero photon energy, we can estimate the high-frequency permittivity  $\epsilon_\infty$  of BP, which is in the  $7 < \epsilon_\infty < 8$  range for all films (Figure S5, Supporting Information). These values are consistent with the empirical band gap–permittivity relationship in III–V semiconductors.<sup>[61]</sup> Since BP is strongly covalent, we expect the static permittivity  $\epsilon_s$  to be nearly equal to  $\epsilon_\infty$ .

### 3.4. Electrical Properties

#### 3.4.1. Intrinsic and Extrinsic Dopants in BP

The origin of the high carrier concentration reported for many BP crystals and films, either p-type<sup>[2,3,5,21,22]</sup> or n-type<sup>[3,5,13,23]</sup> is unclear. First-principles calculations indicate that the lowest-energy acceptor level in BP is the  $P_B$  antisite.<sup>[9]</sup> However, this defect has a deep charge transition level (more than 0.5 eV above the valence band maximum), a high formation energy (≈3.3 eV in the p-type regime, even under favorable B-rich conditions), and is highly compensated by the  $P_B$  donor. A similar situation exists for the dominant  $P_B$  donor under B-rich conditions. It is therefore unlikely that these native defects can be responsible for the carrier concentrations between  $10^{18}$  and  $10^{21}$  cm<sup>−3</sup> observed in most studies of crystalline BP.

Extrinsic defect calculations<sup>[9]</sup> indicate that Si, C, and Be should be more effective substitutional dopants compared to intrinsic defects in BP. All these impurities can dope BP either n-type or p-type depending on whether substitution occurs on the B site (n-type) or on the P site (p-type). Just like the intrinsic defects, B-poor conditions favor n-type conductivity and B-rich conditions favor p-type conductivity.<sup>[9]</sup> Takigawa et al.<sup>[12]</sup> and Kumashiro<sup>[5]</sup> had already hypothesized an “autodoping”

mechanism in BP due to diffusion of Si from the substrate into BP. Substantial Si impurity levels ( $10^{20} \text{ cm}^{-3}$  at  $1050 \text{ }^\circ\text{C}$  growth temperature) were detected in BP by secondary mass ion spectroscopy (SIMS).<sup>[5]</sup> The Si content generally increased with increasing growth temperature and was correlated with the carrier concentration in BP.<sup>[5]</sup> In general, the highest carrier concentrations reported in previous studies (above  $10^{19} \text{ cm}^{-3}$ ) have been achieved in the cases where BP was deposited on a Si-containing substrate and at high temperatures.<sup>[3,13,22]</sup> As another potential source of contamination, we note that the highest purity of elemental boron sources available from commercial suppliers is often only 99.9%. Two different suppliers provided us with boron targets of this overall purity—one with 300 ppm Si, the other with 10 ppm Si. The former target can potentially lead to carrier concentrations up to  $1.3 \times 10^{19} \text{ cm}^{-3}$  just due to its Si impurities.

The effect of possible C impurities on the electrical properties of BP has not been discussed in the experimental literature, although C from organic substances and cleaning agents can easily contaminate growth setups. C impurities in solid material sources (including our B sputter targets) are often not documented due to the very low C sensitivity factor of inductively coupled plasma mass spectrometry (ICP-MS), which is typically used for impurity analysis.<sup>[62]</sup> However, C is known to be a common impurity in elemental boron.<sup>[63,64]</sup>

### 3.4.2. C-Doped BP with Short Post-Annealing

The electrical conductivity of BP films annealed for 30 min with 2.5–2.7 at.% C dopant content is shown in **Figure 5a** as a function of annealing temperature and initial B/P stoichiometry. n-type conductivity is only observed for B-poor films at high annealing temperatures, otherwise the films are p-type. The p-type conductivity increases for increasing B/P ratio, as expected from theory,<sup>[9]</sup> and also with increasing annealing temperature (Figure 5a). The maximum p-type conductivity of  $2.1 \text{ S cm}^{-1}$  is achieved for an annealing temperature of  $1050 \text{ }^\circ\text{C}$  and  $\text{B/P} = 1.3$ . This conductivity value is in the typically reported range for BP single crystals and crystalline films.<sup>[2,5,13,21–23]</sup>

We obtained reliable Hall measurements only on three films annealed at  $1050 \text{ }^\circ\text{C}$  (Figure 5b) using a Hall setup designed for low-mobility samples. These measurements already reveal important differences between our nanocrystalline, C-doped films and previously reported crystalline films. The hole concentration in our B-rich films is well above  $10^{20} \text{ cm}^{-3}$ , significantly higher than in any previous report. As expected, the hole concentration drops by several orders of magnitude when moving from B-rich composition to the nominal  $\text{B/P} = 1$  stoichiometry (Figure 5b). The hole mobility is  $0.27 \text{ cm}^2 \text{ V}^{-1} \text{ s}^{-1}$  near the stoichiometric B/P ratio and it drops by one order of magnitude when moving towards B-rich stoichiometries. An alternative non-contact technique (THz spectroscopy) indicates that the sum of electron and hole mobilities in the nearly stoichiometric BP film is about  $0.4 \text{ cm}^2 \text{ V}^{-1} \text{ s}^{-1}$  (Figure S6, Supporting Information). Due to the very small crystallite size in these films ( $\approx 3 \text{ nm}$ ), we expect THz spectroscopy to be sensitive to the same scattering mechanisms as Hall effect measurements, hence the consistency between the two results. These mobility

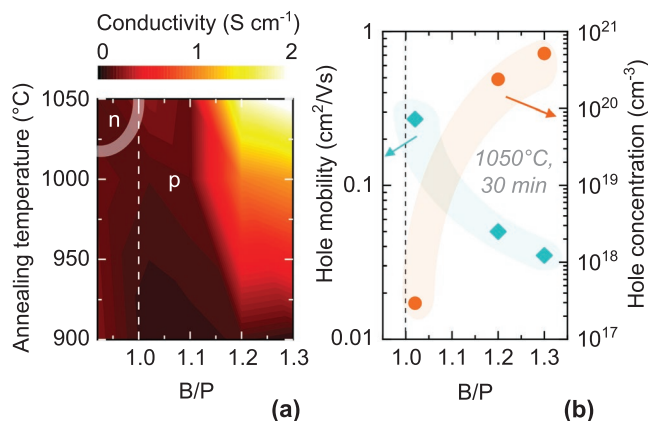


**Figure 5.** Electrical properties of BP. a) Conductivity of C-doped BP films as a function of annealing temperature and initial stoichiometry, with a constant annealing time of 30 min. Only the film with the lowest B/P ratio and annealed at the highest temperature is n-type. The other films are p-type according to Seebeck coefficient measurements. The data points are listed in Table S1, Supporting Information. b) Hole mobility and concentration for three films annealed at  $1050 \text{ }^\circ\text{C}$  as a function of initial composition. No reliable Hall effect measurements were possible for the other films. The shaded regions are guides to the eye.

values are compatible with the only measurement on non-epitaxial, polycrystalline BP that we are aware of ( $0.13 \text{ cm}^2 \text{ V}^{-1} \text{ s}^{-1}$ ).<sup>[26]</sup> Hole mobilities above  $100 \text{ cm}^2 \text{ V}^{-1} \text{ s}^{-1}$  have, however, been demonstrated by several authors on single-crystalline BP.<sup>[3,21]</sup> The low mobility of our stoichiometric film is likely due to the low crystalline quality obtained with short annealing times. The additional decrease in mobility for B-rich stoichiometries may be due to additional ionized impurity scattering from the  $\text{C}_\text{p}$  acceptors and/or to the increased concentration of other crystallographic defects caused by higher nonstoichiometry.

### 3.4.3. C-Doped BP with Long Post-Annealing

The conductivities of films annealed for 24 h with sacrificial P powder and  $\approx 2.5\%$  C doping are in the  $10^{-3}$ – $10^{-2} \text{ S cm}^{-1}$  range regardless of initial stoichiometry. Their conductivity might be underestimated due to a high density of cracks (Figure 3b). Nevertheless, Seebeck coefficients in these films are generally much higher in magnitude than the Seebeck coefficients of the films annealed for a shorter time (**Figure 6a**). Due to the inverse relationship between Seebeck coefficient and carrier concentration, it is then likely that the films annealed for 24 h have much lower carrier concentrations. Another important difference is that films annealed for 24 h have negative Seebeck coefficients, indicating n-type conductivity, unlike the majority of the films annealed for 30 min (Figure 5a). In the following paragraphs we present a hypothesis that could account for the observed differences.

We find that the depth-averaged composition of a BP film after a 30 min anneal at  $950 \text{ }^\circ\text{C}$  changes from  $\text{B/P} = 1.20$  to  $\text{B/P} = 0.99$ . Thus, post-annealing in a P-containing atmosphere tends to compensate the original nonstoichiometry and produces nearly stoichiometric BP ( $\text{B/P} = 1$ ). This compensation process is apparently already completed after 30 min. Yet, the



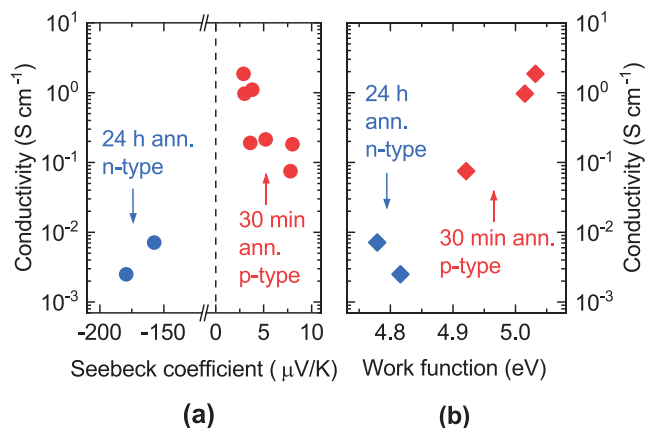


**Figure 6.** a) Seebeck coefficient and b) work function of C-doped BP films with different doping types. Films annealed for 24 h generally have weak n-type doping (large negative Seebeck coefficients). Films annealed for 30 min generally have higher p-type doping (small positive Seebeck coefficients). Despite type inversion, the surface Fermi level (work function) is pinned within a narrow region close to midgap.

measured electrical properties still strongly depend on the B/P ratio of the original as-deposited films (Figure 5). Hence, the high hole concentrations achieved by annealing B-rich BP for a short time can be considered a non-equilibrium property. In the initial stages of the annealing process, both C and P diffuse into B-rich amorphous BP precursors. Under B-rich conditions, formation of  $C_p$  acceptor defects is favorable, causing p-type conductivity. For extended annealing times, B-rich conditions no longer exist so the thermodynamically stable concentration of  $C_p$  acceptors is much lower than the non-equilibrium  $C_p$  concentration achieved in the initial annealing stages. Thus, a significant decrease in the  $C_p$  concentration is expected, but this decrease might take a long time to realize because i) existing B–C bonds have to be broken, and ii) BP becomes more and more crystalline with time, with a corresponding increase of kinetic barriers. As mentioned above, the final defect concentrations achieved after 24 h under our experimental conditions lead to weak n-type conductivity. The likely reason is that BP slowly becomes slightly P-rich in a P-containing atmosphere. This is compatible with the observation of elemental P secondary phases after long annealing times (Figure 3b).

### 3.4.4. Work Function

According to Kelvin probe measurements, the work function of our BP films only spans a limited range (4.75–5.05 eV, Figure 6b), despite the fact that some films annealed for 30 min are degenerately p-type doped and the films annealed for 24 h are n-type. The ionization potential and electron affinity of CVD BP were previously determined as 6.05 and 4.05 eV, respectively, by electrochemical Mott–Schottky measurements.<sup>[65]</sup> Thus, the surface Fermi level of our BP films is pinned around midgap despite their differences in doping type and concentration. Surface Fermi level pinning is a well-known phenomenon in air-exposed III-V semiconductor surfaces. The Fermi level of n-type and p-type GaAs exposed to oxygen is also pinned within a 0.3 eV range around midgap.<sup>[66]</sup> By analogy, we assume that a

high density of surface states due to native oxide formation is responsible for the pinning effect in BP.

### 3.4.5. C versus Si Doping in Sputtered BP

To draw a preliminary comparison between C and Si as potential dopants in BP, we deposited a BP:Si film by reactive cosputtering of a B and a Si target. This film has B/P = 1.11 and a Si content of approximately 2 at.%. Different pieces of this film were annealed for 30 min and co-doped with  $\approx 2.5$  at.% C. We refer to these films as BP:Si,C. P-type conductivity is observed in all the BP:Si,C films after post-annealing. At 1050 °C annealing temperature, the conductivity of BP:Si,C is about the same as the conductivity of a BP:C film with B/P = 1.02 (Figure 7a). The conductivity of all the films (BP:C and BP:Si,C) annealed for 30 min generally has an exponential dependence on annealing temperature (Figure 7a). In Figure 7b, we plot the ratio  $\sigma_{1050}/\sigma_{900}$  between the conductivity obtained after annealing at 1050 °C and after annealing at 900 °C, as a function of the B/P ratio. This quantity is a measure of the conductivity increase with increasing annealing temperature. For BP:C films,  $\sigma_{1050}/\sigma_{900}$  increases with increasing B/P ratio (Figure 7b). For the BP:Si,C series,  $\sigma_{1050}/\sigma_{900}$  is much higher than expected for a BP:C film of the same B/P ratio (Figure 7b).

A possible interpretation of the generally increasing conductivity with annealing temperature is dopant activation, that is, the thermally activated incorporation of  $C_p$  and  $Si_p$  acceptors in the BP lattice. The observation that the Si-codoped films are the least conductive at low annealing temperature could be rationalized by assuming that  $Si_p$  defects form more easily than  $C_p$  defects, (hence, they are more abundant at lower temperatures) but that they are less easily ionized by electrons in the valence

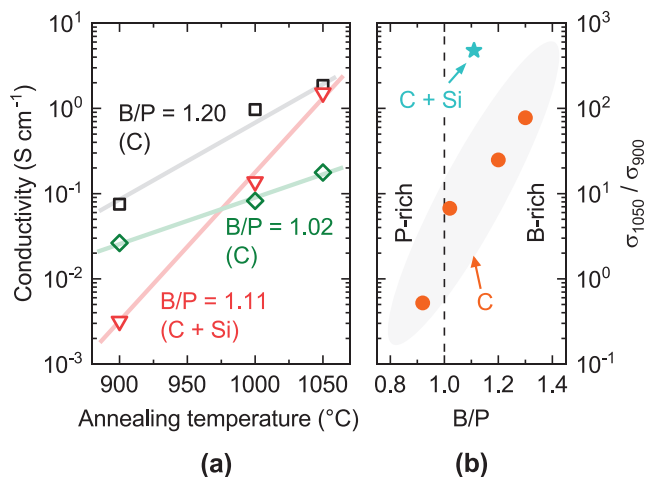


**Figure 7.** Trends in the electrical properties of BP. a) Conductivity of BP:Si,C films as a function of annealing temperature. The conductivity of two BP:C films is shown for comparison (same data as in Figure 5a). In all film series, the conductivity has an approximately exponential dependence on annealing temperature. b) Ratio between the conductivity at the highest annealing temperature ( $\sigma_{1050}$ ) and at the lowest annealing temperature ( $\sigma_{900}$ ). All data points used to plot these figures are listed in Table S1, Supporting Information.

band. With this hypothesis,  $\text{Si}_\text{P}$  defects would yield a lower concentration of free holes at room temperature compared to an equivalent concentration of  $\text{C}_\text{P}$  defects. In fact, this is exactly what was found by first-principles defect calculations.<sup>[9]</sup> The  $\text{C}_\text{P}$  acceptor has a higher formation enthalpy than  $\text{Si}_\text{P}$  at fixed chemical potential (3.0 vs 1.7 eV). However,  $\text{C}_\text{P}$  has a much shallower level than  $\text{Si}_\text{P}$  (0.03 vs 0.12 eV above the valence band maximum).

#### 4. Discussion

It is relatively straightforward to deposit smooth, amorphous BP in a wide range of compositions by reactive sputtering. Nevertheless, this processing route has some disadvantages with respect to CVD. First, B is a very hard element with a much lower sputter yield than the soft metals used in n-type TCMs (e.g., Zn, In, Sn). Since high sputter powers are not viable due to the low thermal conductivity of B, low deposition rates in reactive sputtering of B seem unavoidable. A BP compound target is also expected to have a low sputter yield and is not typically offered by commercial suppliers. Nevertheless, it may allow for higher powers due the high thermal conductivity of BP.<sup>[1]</sup> A potential advantage of reactively sputtered BP is that the as-deposited amorphous films have a relatively low surface roughness of around 2 nm RMS for 100–200-nm-thick films (Table S2, Supporting Information). BP has been proposed as a material for extreme UV optics but the large roughness of CVD films was found to be a limiting factor.<sup>[8]</sup> Thus, reactive sputtering may be a more promising route for this particular application.

Nanocrystalline BP films with small ( $\approx 3$  nm) crystallite size are not sufficiently transparent for TCM applications due to strong absorption above their nominally indirect band gap. High crystalline quality is thus an important requirement for BP and for other candidate TCMs with indirect gaps in the visible. This requirement is much less stringent in direct-gap n-type oxide TCMs, which often have very small grain sizes.<sup>[34,38]</sup> Unfortunately, reactively sputtered BP films on fused silica are still amorphous even at a substrate temperature of 800 °C. The crystallinity of BP films can be improved by post-annealing in a P-containing atmosphere but the crystallite size seems to be limited by the particle size of the as-deposited films, without significant coalescence between these particles. The limiting crystallite size obtained by long anneals at high temperatures is in the 30–40 nm range. This crystallite size might be sufficient to prevent strong indirect absorption, but we could not draw any conclusion in this regard because our crystalline films have spurious phases at the surface (Figure 3b). Significant light scattering from these phases, as well as their unknown optical properties, makes it difficult to determine the intrinsic absorption coefficient of the underlying BP film.

With short annealing times, very high hole concentrations can be achieved in nanocrystalline BP under B-rich conditions using extrinsic dopants. Higher hole concentrations are realized with C dopants than with Si dopants, probably because  $\text{C}_\text{P}$  is significantly shallower than  $\text{Si}_\text{P}$ . Since the conductivity of BP films without extrinsic doping was below  $10^{-3}$  S  $\text{cm}^{-1}$  under all the conditions investigated in this study, we believe that some

of the previously reported high carrier concentrations in BP may be due to Si and/or C incorporation from the substrate or other sources.

Long annealing times have the advantage of better BP crystalline quality and the potential for higher optical transmission. However, we encountered three issues. First, a higher density of cracks (Figure 3b). Second, formation of secondary phases which we identified as elemental phosphorus (Figure S3, Supporting Information). Third, the tendency of B-rich films to reach their stoichiometric B/P ratio by incorporating P from the evaporated P powder (Section 3.4.3). This tendency limits the achievable hole concentration, because acceptor defects have higher formation energies under stoichiometric conditions. The issue with cracks might be addressed by a different substrate with a higher thermal expansion coefficient. The two other issues could be addressed by optimizing the amount of sacrificial P powder and employing a thermal gradient to avoid condensation of excess P on the BP films. An annealing system with a continuous  $\text{PH}_3$  flow might be a more practical solution to control P incorporation in the film.

#### 5. Conclusion and Outlook

Amorphous BP films can be deposited by reactive sputtering in a wide range of compositions. However, they require a post-annealing step at 1000 °C or above in a P-containing atmosphere for crystallization and dopant activation. Our study points to C as a more effective p-type dopant than either Si or native defects in BP. Incorporation of 2.5% C in BP led to the highest hole concentration reported to date for p-type BP ( $5 \times 10^{20}$   $\text{cm}^{-3}$ ). While an initial B-rich composition generally favors p-type conductivity, it was also possible to obtain n-type conductivity in B-poor films. Thus, we confirm that BP is amenable to bipolar doping, a rare feature in wide band gap materials. The properties of BP films appear to be stable under ambient conditions.

The hole mobilities and optical transmission of our films were too low for TCM applications. The most likely cause is the relatively poor crystalline quality of BP films annealed for a relatively short time. In general, incomplete crystallization will penalize any candidate transparent conductor with an indirect gap in the visible. The reason is that participation of phonons in indirect transitions is not required in the absence of long-range order, so the absorption coefficient will increase with respect to the case of a perfect crystal. It may be possible to improve the optoelectronic properties through longer anneals with optimized process parameters. Nevertheless, single-step, high-temperature deposition processes at higher P partial pressures are more likely to achieve higher crystalline quality and seem to be a more practical solution in general. Based on previously reported mobilities and absorption coefficient in crystalline BP, as well as the high hole concentrations demonstrated in this study, we argue that BP:C has the potential to achieve high TCM figures of merit and certainly deserves further investigation. Depositing C-doped BP by CVD using, for example, a  $\text{CH}_4$  doping source, might be a promising strategy. In particular, it will be important to clarify if nonepitaxial, polycrystalline BP can achieve similar hole mobilities and optical transparency as single-crystalline films.



High process temperatures seem unavoidable for obtaining high crystalline quality and dopant incorporation in BP, so it is likely that BP TCMs can only find applications as the first layer in a device stack. Still, a TCM on a transparent substrate is the initial layer in many important optoelectronic devices, such as CdTe and perovskite solar cells,<sup>[67,68]</sup> so device applications are in principle possible. Since post-annealed BP films on fused silica substrates are prone to cracking, alternative refractory and transparent substrates with a higher thermal expansion coefficient might be necessary. BP is itself a refractory material, and this property could be particularly useful as a transparent contact in thin-film optoelectronic technologies requiring high-temperature processing in other functional layers, such as the emerging class of chalcogenide perovskites.<sup>[69]</sup> As an additional advantage, the thermal conductivity of BP is among the highest known for any material.<sup>[1]</sup> In bifacial solar cells lacking a continuous metallic contact and only consisting of materials with low thermal conductivity, BP contacts could have an additional thermal management function. Finally, the possibility of bipolar doping is encouraging for possible applications in transparent electronics.

## 6. Experimental Section

**Film Deposition:** Amorphous BP films were deposited on fused silica and crystalline Si substrates by reactive radio-frequency (RF) magnetron sputtering of B targets in an Ar/PH<sub>3</sub> atmosphere. The desired Ar/PH<sub>3</sub> ratio was obtained by tuning the relative flow rate of a diluted PH<sub>3</sub> source (5% in Ar) and a pure Ar source. Due to the very low sputter yield of B, the films were grown under simultaneous sputtering of two 2" B targets from separate magnetron sources, unless otherwise specified. A bare 0.25"-thick B target (99.9% purity, Kurt J. Lesker) and a 0.125"-thick B target In-bonded to a Cu backing plate (99.9% purity, Advanced Engineering Materials) were used. The two targets were confocally oriented with respect to the middle of the substrate. The gas inlet inside the deposition chamber was at approximately the same distance from the two targets and from the substrate. The substrates were clamped to a metallic platen, which was heated by infrared lamps. The quoted temperatures are those measured on the metallic platen after the 30 min stabilization time that preceded each deposition. The BP films employed for post-annealing experiments were deposited at room temperature with a total pressure of 5 mTorr, a PH<sub>3</sub> partial pressure in the 0.02–0.06 mTorr range, an RF power of 40 W for each target, and a target–substrate distance of 10cm. Safety precautions adopted when working with PH<sub>3</sub> included gas dilution, continuous PH<sub>3</sub> level monitoring at different locations, interlocks, PH<sub>3</sub> pumping and scrubbing, and wearing self-contained breathing apparatus when opening the sputter chamber. A more detailed description is available elsewhere.<sup>[70]</sup>

**Post-Annealing:** Ampoules for annealing treatments were made from 1220 mm long, 12 mm outer diameter, and 2 mm wall thickness fused silica tubing (Technical Glass Products, OH, USA). The tubes were cut into 400 mm sections using a diamond saw. The open-ended 400 mm tube sections were rinsed using water followed by isopropyl alcohol to remove any residual water. Tube sections were then dried using dry compressed air. An oxy-propylene torch was used to pull the 400 mm tube sections into half-ampoules (200 mm sections with a single closed end). As-deposited BP films were cut into 7 × 12 mm<sup>2</sup> pieces for post-annealing. Two such samples were placed in each half-ampoule. Care was taken to ensure that there was no overlap between the two samples inside of the ampoules. Unless otherwise specified, samples were annealed in a P-containing atmosphere by loading sacrificial red phosphorus powder (3 mg) in the ampoule. Ampoules were then sealed in vacuum after three evacuation (<100 mTorr) and purging (Ar) cycles, with a final sealed ampoule length of 120 mm. Under these conditions,

the total phosphorus pressure at 1000 °C was estimated as 500 Torr and was expected to consist of gaseous P<sub>4</sub> and P<sub>2</sub> species in approximately equal concentrations.<sup>[71]</sup> For the annealing experiments without P powder, the ampoules were sealed under 400 Torr of Ar after the last evacuation step. The ampoules were placed horizontally in a tube furnace (Thermcraft Inc., NC, USA) as close to the control thermocouple as possible. A fixed heating and cooling ramp rate of 20 °C min<sup>-1</sup> was used while the soak time and temperatures were changed as a variable.

**Characterization:** X-ray diffraction measurements were conducted with a Bruker D8 diffractometer using Cu K<sub>α</sub> radiation and a 2D detector. To cover the desired 2θ range, three frames were collected with the incidence angle ω fixed at 10°, 22.5°, and 35° and the detector center fixed at 2θ values of 35°, 60°, and 85°, respectively. The diffraction intensity at each 2θ angle was integrated over the χ range measured by the 2D detector. Structural analysis by XRD was complemented by Raman spectroscopy (Renishaw inVia) at 532 nm excitation and 40 W mm<sup>-2</sup> power density.

Film composition was determined by AES (Physical Electronics 710 scanning Auger nanoprobe) with a 10 kV, 10 nA primary beam and after removing the native oxide and adsorbed species with an Ar<sup>+</sup> beam (2 kV). The default sensitivity factors for numerically differentiated B-KLL and P-LMM peaks were used for quantification, which was performed using Physical Electronics MultiPak v9.6.1.7. Unless otherwise specified, the B/P ratios quoted in the article refer to atomic composition of the films before annealing. SEM images were taken with a Hitachi S-3400N instrument with a field emission gun and 5 kV beam voltage.

Film thickness and optical properties were determined by variable-angle spectroscopic ellipsometry measurements using a J.A. Woollam Co. M-2000 rotating-compensator ellipsometer. Ellipsometry spectra were fitted with a substrate/film/roughness layer model in the CompleteEase software (J.A. Woollam). The fitting parameters were the thicknesses of the film and roughness layers, as well as the dielectric function of the film layer. The latter was represented by a Kramers–Kronig-consistent b-spline function with 0.3 nodes per eV. Optical transmission in the visible and near IR was measured in a home-built setup.

Electrical conductivity was measured on the plane of the substrate by a collinear four-point probe. Hall carrier concentration and mobility were measured with a Hall measurement station for low-mobility samples (FastHall, LakeShore Cryotronics) in the van der Pauw configuration. The results were validated by reversing the magnetic field and changing the measurement current. In case of inconsistencies, the results were discarded. The ellipsometry-determined film thickness was used in the derivation of the electrical properties.

The Seebeck coefficient was measured in a home-built setup using In contacts and four temperature differences in the vicinity of room temperature. After checking that the thermovoltage depended linearly on the temperature difference, the Seebeck coefficient of BP was determined as the slope of the linear curve minus the Seebeck coefficient of the In contacts. The work function was measured with a SKP SPV LE 450 Kelvin probe (KP Technology) calibrated with a standard Au sample.

## Supporting Information

Supporting Information is available from the Wiley Online Library or from the author.

## Acknowledgements

This project has received funding from the European Union's Horizon 2020 research and innovation programme under the Marie Skłodowska-Curie grant agreement No 840751 (synthesis, characterization, and analysis work). This work was authored in part at the National Renewable Energy Laboratory, operated by Alliance for Sustainable Energy, LLC, for the U.S. Department of Energy

(DOE) under Contract No. DE-AC36-08GO28308. Funding supporting development and operation of synthesis and characterization equipment (A.C.T., R.R.S., A.Z.) was provided by the Office of Science, Office of Basic Energy Sciences. J.M.A. and E.S.T. acknowledge NSF DMR award 1555340. A.C. thanks Joel Basile Varley and Geoffroy Hautier for useful discussions.

Open access funding enabled and organized by Projekt DEAL.

## Conflict of Interest

The authors declare no conflict of interest.

## Data Availability Statement

The data that support the findings of this study are openly available at the following URL: <https://hitem.nrel.gov/> (doi: <https://doi.org/10.7799/1407128>).

## Keywords

bipolar doping, boron phosphide, phosphides, p-type transparent conductors, sputtering

Received: January 6, 2022

Revised: January 28, 2022

Published online: February 27, 2022

- [1] J. S. Kang, H. Wu, Y. Hu, *Nano Lett.* **2017**, *17*, 7507.
- [2] B. Stone, D. Hill, *Phys. Rev. Lett.* **1960**, *4*, 282.
- [3] K. Shohno, M. Takigawa, T. Nakada, *J. Cryst. Growth* **1974**, *24-25*, 193.
- [4] D. S. Ginley, R. J. Baughman, M. A. Butler, *J. Electrochem. Soc.* **1983**, *130*, 1999.
- [5] Y. Kumashiro, *J. Mater. Res.* **1990**, *5*, 2933.
- [6] L. Shi, P. Li, W. Zhou, T. Wang, K. Chang, H. Zhang, T. Kako, G. Liu, J. Ye, *Nano Energy* **2016**, *28*, 158.
- [7] S. Mou, T. Wu, J. Xie, Y. Zhang, L. Ji, H. Huang, T. Wang, Y. Luo, X. Xiong, B. Tang, X. Sun, *Adv. Mater.* **2019**, *31*, 1903499.
- [8] S. P. Huber, V. V. Medvedev, J. Meyer-Ilse, E. Gullikson, B. Padavala, J. H. Edgar, J. M. Sturm, R. W. E. van de Kruijs, D. Prendergast, F. Bijkerk, *Opt. Mater. Express* **2016**, *6*, 3946.
- [9] J. B. Varley, A. Miglio, V.-A. Ha, M. J. van Setten, G.-M. Rignanese, G. Hautier, *Chem. Mater.* **2017**, *29*, 2568.
- [10] A. N. Fioretti, M. Morales-Masis, *J. Photonics Energy* **2020**, *10*, 042002.
- [11] J. Willis, D. O. Scanlon, *J. Mater. Chem. C* **2021**, *9*, 11995.
- [12] M. Takigawa, M. Hirayama, K. Shohno, *Jpn. J. Appl. Phys.* **1974**, *13*, 411.
- [13] M. Iwami, T. Tohda, K. Kawabe, *Electr. Eng. Jpn.* **1975**, *95*, 19.
- [14] R. J. Archer, R. Y. Koyama, E. E. Loebner, R. C. Lucas, *Phys. Rev. Lett.* **1964**, *12*, 538.
- [15] V.-A. Ha, B. Karasulu, R. Maezono, G. Brunin, J. B. Varley, G.-M. Rignanese, B. Monserrat, G. Hautier, *Phys. Rev. Mater.* **2020**, *4*, 065401.
- [16] M. K. Svendsen, H. Sugimoto, A. Assadillayev, D. Shima, M. Fujii, K. S. Thygesen, S. Raza, <http://arxiv.org/abs/2112.13600> (accessed: January 2022)
- [17] E. Schroten, A. Goossens, J. Schoonman, *J. Appl. Phys.* **1998**, *83*, 1660.
- [18] A. Zunger, *Appl. Phys. Lett.* **2003**, *83*, 57.
- [19] A. Goyal, P. Gorai, S. Anand, E. S. Toberer, G. J. Snyder, V. Stevanović, *Chem. Mater.* **2020**, *32*, 4467.
- [20] R. G. Gordon, *MRS Bull.* **2000**, *25*, 52.
- [21] C. C. Wang, M. Cardona, A. G. Fischer, *RCA Rev.* **1964**, *25*, 2.
- [22] T. L. Chu, J. M. Jackson, A. E. Hyslop, S. C. Chu, *J. Appl. Phys.* **1971**, *42*, 420.
- [23] N. Kato, W. Kammura, M. Iwami, K. Kawabe, *Jpn. J. Appl. Phys.* **1977**, *16*, 1623.
- [24] A. Crovetto, H. Hempel, M. Rusu, L. Choubrac, D. Kojda, K. Habicht, T. Unold, *ACS Appl. Mater. Interfaces* **2020**, *12*, 48741.
- [25] M. Odawara, T. Udagawa, G. Shimaoka, *Jpn. J. Appl. Phys.* **2005**, *44*, 681.
- [26] A. Goossens, E. M. Kelder, J. Schoonman, *Ber. Bunsen-Ges. Physik. Chem.* **1989**, *93*, 1109.
- [27] C. Yang, M. Kneiß, M. Lorenz, M. Grundmann, *Proc. Natl. Acad. Sci. U. S. A.* **2016**, *113*, 12929.
- [28] K. Woo, K. Lee, K. Kovnir, *Mater. Res. Express* **2016**, *3*, 074003.
- [29] Y. Kumashiro, T. Yokoyama, T. Sakamoto, T. Fujita, *J. Solid State Chem.* **1997**, *133*, 269.
- [30] E. Schroten, A. Goossens, J. Schoonman, *J. Electrochem. Soc.* **1999**, *146*, 2045.
- [31] S. Dalui, S. Hussain, S. Varma, D. Paramanik, A. Pal, *Thin Solid Films* **2008**, *516*, 4958.
- [32] S. Yoshioka, F. Oba, R. Huang, I. Tanaka, T. Mizoguchi, T. Yamamoto, *J. Appl. Phys.* **2008**, *103*, 014309.
- [33] A. Bikowski, M. Rengachari, M. Nie, N. Wanderka, P. Stender, G. Schmitz, K. Ellmer, *APL Mater.* **2015**, *3*, 060701.
- [34] M. Morales-Masis, S. De Wolf, R. Woods-Robinson, J. W. Ager, C. Ballif, *Adv. Electron. Mater.* **2017**, *3*, 1600529.
- [35] B. Szyszka, in *Transparent Conductive Zinc Oxide: Basics and Applications in Thin Film Solar Cells*, (Eds: K. Ellmer, A. Klein, B. Rech), Springer, Berlin **2008**, p. 221.
- [36] H.-S. Seo, W. Cao, J. C. Xiao, Y.-C. Wu, B. Zhao, X. ZHANG, X. Yan, *SID Symp. Dig. Tech. Pap.* **2020**, *51*, 301.
- [37] Z. Jia, J. Zhu, C. Jiang, W. Shen, J. Han, R. Chen, *Appl. Surf. Sci.* **2011**, *258*, 356.
- [38] A. Crovetto, T. S. Ottsen, E. Stamate, D. Kjær, J. Schou, O. Hansen, *J. Phys. D: Appl. Phys.* **2016**, *49*, 295101.
- [39] K. Utsumi, H. Iigusa, R. Tokumaru, P. Song, Y. Shigesato, *Thin Solid Films* **2003**, *445*, 229.
- [40] H. Xia, Q. Xia, A. L. Ruoff, *J. Appl. Phys.* **1993**, *74*, 1660.
- [41] B. Morosin, A. W. Mullendore, D. Emin, G. A. Slack, in *AIP Conference Proceedings*, vol. 140, AIP **1986**, pp. 70–86. <https://aip.scitation.org/doi/abs/10.1063/1.35589>
- [42] V. L. Solozhenko, O. O. Kurakevych, Y. Le Godec, A. V. Kurnosov, A. R. Oganov, *J. Appl. Phys.* **2014**, *116*, 033501.
- [43] K. Nakamura, M. Fujitsuka, M. Kitajima, *Phys. Rev. B* **1990**, *41*, 12260.
- [44] G. Fasol, M. Cardona, W. Hönlle, H. von Schnering, *Solid State Commun.* **1984**, *52*, 307.
- [45] U. Kuhlmann, H. Werheit, T. Lundström, W. Robers, *J. Phys. Chem. Solids* **1994**, *55*, 579.
- [46] T. H. de Keijser, J. I. Langford, E. J. Mittemeijer, A. B. P. Vogels, *J. Appl. Crystallogr.* **1982**, *15*, 308.
- [47] B. Padavala, H. Al Atabi, L. Tengdelius, J. Lu, H. Högberg, J. Edgar, *J. Cryst. Growth* **2018**, *483*, 115.
- [48] M. Ruck, D. Hoppe, B. Wahl, P. Simon, Y. Wang, G. Seifert, *Angew. Chem., Int. Ed.* **2005**, *44*, 7616.
- [49] W. Hittorf, *Annal. Phys. Chem.* **1865**, *202*, 193.
- [50] S. Motojima, S. Yokoe, K. Sugiyama, *J. Cryst. Growth* **1980**, *49*, 1.
- [51] E. Schroten, A. Goossens, J. Schoonman, *J. Appl. Phys.* **1996**, *79*, 4465.
- [52] G. A. Slack, S. F. Bartram, *J. Appl. Phys.* **1975**, *46*, 89.
- [53] E. A. Davis, N. F. Mott, *Philos. Mag.* **1970**, *22*, 0903.
- [54] G. E. Jellison, M. F. Chisholm, S. M. Gorbatskin, *Appl. Phys. Lett.* **1993**, *62*, 3348.

- [55] S. Bolat, M. Durandurdu, *J. Non-Cryst. Solids* **2021**, 570, 121006.
- [56] N. Morita, A. Yamamoto, *Jpn. J. Appl. Phys.* **1975**, 14, 825.
- [57] W. Wetzling, J. Windscheif, *Solid State Commun.* **1984**, 50, 33.
- [58] R. Swanepoel, *J. Phys. E: Sci. Instrum.* **1984**, 17, 896.
- [59] A. Crovetto, A. Cazzaniga, R. B. Ettliger, J. Schou, O. Hansen, *Sol. Energy Mater. Sol. Cells* **2018**, 187, 233.
- [60] A. Crovetto, A. Cazzaniga, R. B. Ettliger, J. Schou, O. Hansen, *Thin Solid Films* **2015**, 582, 203.
- [61] N. N. Sirota, in *Semiconductors and Semimetals*, Vol. 4, Elsevier, Amsterdam **1968**, p. 156.
- [62] R. S. Houk, *Anal. Chem.* **1986**, 58, 97A.
- [63] N. N. Greenwood, A. Earnshaw, *Chemistry of the Elements*, 2nd ed., Butterworth-Heinemann, Oxford **1997**.
- [64] D. Yu, C. Kong, J. Zhuo, S. Li, Q. Yao, *Sci. China Technol. Sci.* **2015**, 58, 2016.
- [65] A. Goossens, E. M. Kelder, R. J. M. Beeren, C. J. G. Bartels, J. Schoonman, *Ber. Bunsen-Ges. Physik. Chem.* **1991**, 95, 503.
- [66] W. E. Spicer, I. Lindau, P. Skeath, C. Y. Su, P. Chye, *Phys. Rev. Lett.* **1980**, 44, 420.
- [67] R. Woods-Robinson, T. Ablekim, A. Norman, S. Johnston, K. A. Persson, M. O. Reese, W. K. Metzger, A. Zakutayev, *ACS Appl. Energy Mater.* **2020**, 3, 5427.
- [68] M. Saliba, J.-P. Correa-Baena, C. M. Wolff, M. Stolterfoht, N. Phung, S. Albrecht, D. Neher, A. Abate, *Chem. Mater.* **2018**, 30, 4193.
- [69] A. Crovetto, R. Nielsen, M. Pandey, L. Watts, J. G. Labram, M. Geisler, N. Stenger, K. W. Jacobsen, O. Hansen, B. Seger, I. Chorkendorff, P. C. K. Vesborg, *Chem. Mater.* **2019**, 31, 3359.
- [70] R. R. Schnepf, A. Crovetto, P. Gorai, A. Park, M. Holtz, K. N. Heinselman, S. R. Bauers, M. Brooks Tellekamp, A. Zakutayev, A. L. Greenaway, E. S. Toberer, A. C. Tamboli, *J. Mater. Chem. C* **2022**, 10, 870.
- [71] H. Bock, H. Mueller, *Inorg. Chem.* **1984**, 23, 4365.